Clim. Past, 20, 2741–2758, 2024
https://doi.org/10.5194/cp-20-2741-2024

Climate of the Past
Open Access
EGU

Improving the age constraints on the archeological record in Scladina Cave (Belgium): new speleothem U–Th ages

Hubert B. Vonhof[1], Sophie Verheyden[2], Dominique Bonjean[3], Stéphane Pirson[4,5], Michael Weber[6], Denis Scholz[6], John Hellstrom[7], Hai Cheng[8,9], Xue Jia[8], Kévin Di Modica[3], Gregory Abrams[3,10], Marjan A. P. van Nunen[11], Joost Ruiter[11], Michèlle van der Does[12], Daniel Böhl[6], and Jeroen H. J. L. van der Lubbe[11]

[1]Max Planck Institute for Chemistry, Mainz, Germany
[2]Royal Belgian Institute of Natural Sciences, Brussels, Belgium
[3]Scladina Cave Archeological Centre, Espace muséal d'Andenne, Andenne, Belgium
[4]Wallonia Heritage Agency, Scientific and Technical Direction, Namur, Belgium
[5]Department of Geology and European Archaeometry Centre, University of Liège, Liège, Belgium
[6]Institute for Geosciences, Johannes Gutenberg University, Mainz, Germany
[7]School of Geography, Earth and Atmospheric Sciences, University of Melbourne, Melbourne, Australia
[8]Institute of Global Environmental Change, Xi'an Jiaotong University, Xi'an 710054, China
[9]Institute of Earth Environment, Chinese Academy of Sciences, Xi'an 710061, China
[10]Department of Archaeology, ArcheOS – Research Laboratory for Biological Anthropology, Ghent University, Ghent, Belgium
[11]Institute of Earth Sciences, Vrije Universiteit Amsterdam, Amsterdam, the Netherlands
[12]Alfred Wegener Institute, Helmholtz Centre for Polar and Marine Research, Bremerhaven, Germany

Correspondence: Hubert B. Vonhof (hubert.vonhof@mpic.de)

Received: 2 April 2024 – Discussion started: 16 April 2024
Revised: 29 August 2024 – Accepted: 27 September 2024 – Published: 19 December 2024

Abstract. The sedimentary sequence in Scladina Cave (Belgium) is well-known for its rich Middle Paleolithic assemblages and its numerous faunal remains. Of particular interest is the presence of a nearly complete mandible of a Neanderthal child. To place all of these finds into the correct chronostratigraphic context, various dating techniques have been applied over the past decades. This resulted in a reasonably well-constrained age model, roughly spanning the last glacial cycle. Age constraints of the lower part of the Scladina sequence as well as from the underlying Sous-Saint-Paul Cave were, however, absent until now. Previous attempts to date several speleothem layers in Scladina Cave using U–Th dating were only partly successful, presumably because diagenetic alteration of speleothem material compromised the ages. In the present study we reassessed U–Th dating of various speleothem levels in Scladina Cave, applying state-of-the-art U–Th dating and carefully selecting material that experienced little to no diagenetic alteration. The new results constitute a robust age framework for the Scladina sequence, which provides precisely dated stratigraphic anchor points that improve the previous age model. Furthermore, new U–Th analyses for speleothems from the lower part of the Scladina sequence and from the Sous-Saint-Paul sequence document Middle Pleistocene ages, making this one of the longer fossil-rich cave sedimentary sequences in NW Europe. The new data confirm that speleothem growth predominantly took place in periods of warmer climate, while siliciclastic sediments characterize the colder intervals. New speleothem ages further suggest that the Neanderthal mandible found in the sequence and previously placed in Marine Isotope Stage 5a or 5b could potentially be as old as Marine Isotope Stage 5d.

1 Introduction

Scladina Cave is situated near the Belgian town of Sclayn in a valley branching off the Meuse River (Fig. 1). The cave has been investigated since 1971, following the discovery of Middle Paleolithic artifacts at the entrance of the cave (Bonjean et al., 2014). The cave at that time was nearly completely filled with a stack of siliciclastic sediments and intercalated flowstone levels. After several decades of careful scientific excavation, a significant part of the sedimentary infill has been excavated (Fig. 2), and the cave continues to deliver a wealth of archeological and paleontological information (Bonjean et al., 2014).

Arguably the most significant fossils retrieved from the cave are a mandible, a fragment of right maxillary, and 16 teeth of a juvenile Neanderthal (Bonjean et al., 1996; Otte et al., 1993; Toussaint and Bonjean, 2014). Owing to careful excavation methods and favorable conditions for the preservation of ancient DNA in Scladina Cave, it has been possible to extract valuable genomic information from the mandible (Orlando et al., 2006; Peyregne et al., 2019). Besides this Neanderthal material, a wealth of artifacts (stone tools) and fossil faunal remains have been retrieved from the sedimentological sequence in the cave (Bonjean et al., 2014; Otte, 1992), and geochemical analyses on that material have provided valuable insight into the paleoenvironmental and paleoecological setting (Bocherens et al., 1997; Bocherens, 2014).

The chronostratigraphic context of the finds from the cave has been reconstructed using a variety of dating techniques anchored in meticulous reconstruction of the lithostratigraphy and sedimentary dynamics (Bonjean, 1998; Pirson, 2007, 2014; Pirson et al., 2014b, 2008). The dating technique that is often most reliable in cave settings, uranium series dating of speleothem $CaCO_3$, however, did not initially yield very precise ages (Bonjean, 1998; Gewelt et al., 1992). Presumably this was due to diagenetic alteration of speleothem calcite, as most speleothem material has been buried in siliciclastic sediments in Scladina Cave, and degradation of speleothem calcite is commonly observed in the excavated material.

Summarizing all of the dating efforts done so far, a consistent age model is available for the spatially complex Scladina Cave infill stratigraphy (Pirson, 2014; Pirson et al., 2014b). In that age model, flowstone levels separating the different siliciclastic stratigraphic units generally seem to represent the warmer climate periods through the last glacial cycles, as is also the case in other caves in Belgium (Quinif, 2006). However, the accuracy of the existing age model for Scladina has not been easy to establish, as the dating methods used have significant uncertainties, some parts of the sedimentary infill are difficult to date, and some discrepancies between age estimates remain (Pirson et al., 2014b). Furthermore, the age model of the lower part of the sequence, including the sediments in the underlying Sous-Saint-Paul Cave, is essentially unknown.

In the present paper, we have reinvestigated the potential for uranium series dating of speleothem material in Scladina Cave. This is done because significant progress has been made in U–Th dating of speleothem material over the past decades. The advent of multi-collector inductively coupled plasma mass spectrometry (MC-ICP-MS) in particular has enabled more precise analysis of U and Th on smaller samples than was previously possible (Cheng et al., 2013; Scholz and Hoffmann, 2008). Furthermore, new and better-preserved speleothem material has been excavated from the cave. The objective of this study was to carefully select the best-preserved flowstone and stalagmite material in the cave. In doing so, we targeted all known speleothem levels that were thick enough to preserve good-quality speleothem calcite. We included two flowstone levels from the Sous-Saint-Paul Cave, the sediments of which stratigraphically underlie Scladina Cave (Otte, 1992; Pirson et al., 2008).

In addition to our dating efforts, we used laser ablation ICP-MS elemental analysis on the speleothem material to characterize the diagenetic state of the material.

2 Materials and methods

2.1 Speleothem sample collection

The current stratigraphic profile of the sediment infill of Scladina Cave, including the sediments from the underlying Sous-Saint-Paul Cave, is shown in Fig. 3. It contains several levels with speleothem material, the most prominent of which are the currently active speleothems growing on top of unit H. From this level we collected two stalagmites and a column for analysis. A single speleothem was collected from layer 1B-BK (in unit 1B-BRUN). Two more stalagmites were collected from another prominent speleothem growth interval in unit 4A, previously dated to Marine Isotope Stage (MIS) 5: one is coming from an in situ speleothem (CC4 in unit 4A-IP), while the other one consists of two halves of a stalagmite reworked from CC4 in a gully (unit 4A-CHE). From a speleothem complex in stratigraphic unit 6B, we collected two stalagmites, and from two more speleothem levels in Sous-Saint-Paul Cave, covering the lowermost part of the composite sequence, we cut flowstone fragments. Slabs prepared from the samples collected are shown in Fig. A1. Standard petrographic thin sections of selected samples were cut and polished from these slabs.

2.2 U series analysis

The $^{230}Th/U$ dating of the selected material was performed over a period of several years in four different laboratories. In all laboratories, samples were dissolved in nitric acid before adding a mixed ^{229}Th–^{233}U–^{236}U spike solution and separating U and Th using ion exchange columns. The spike solutions were independently calibrated in the corresponding

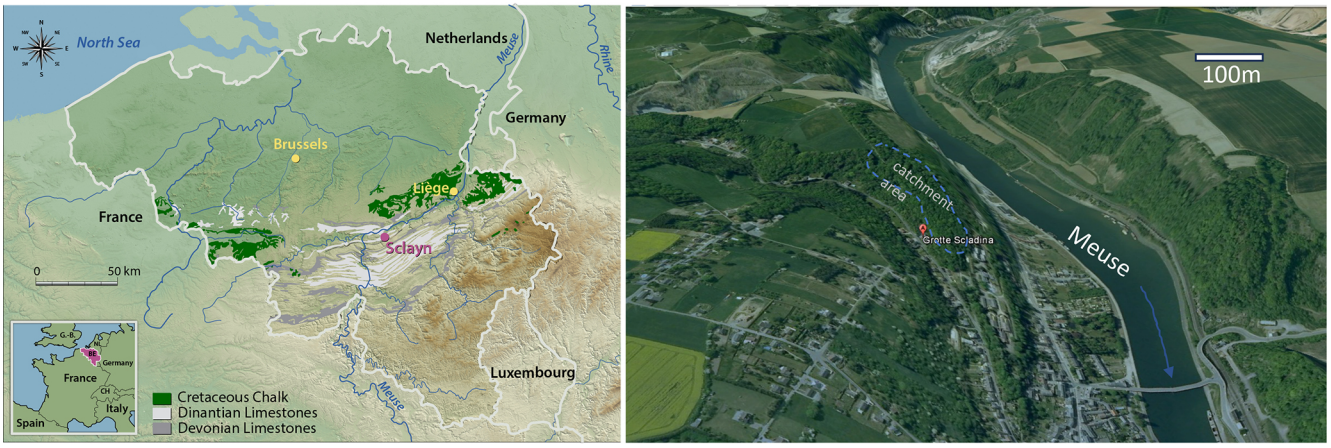

Figure 1. The left-hand panel shows a map of Belgium with the town Sclayn, where Scladina Cave is situated, marked in magenta (Basemap © K. di Modica). The right-hand panel shows an aerial view of Scladina Cave, taken from the perspective of the Pontine valley (source: © Google Earth, with Landsat/Copernicus image). Our rough approximation of the catchment area of dripwater in the cave is shown in blue.

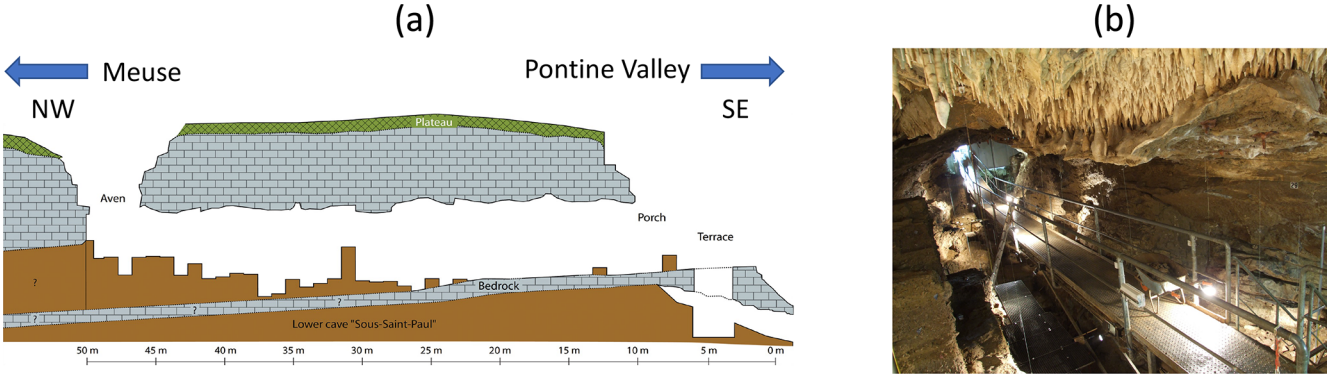

Figure 2. **(a)** Schematic cross section of Scladina Cave and the underlying Sous-Saint-Paul Cave (Bonjean et al., 2014). The entrance at the SE side is nowadays closed by a door. **(b)** Scaffolding and walkways installed in the cave, with positioning lines that mark the archeological excavation grid also shown. The irregular cave sediment depth (brown) represents the ongoing archeological excavation activity. The lower Sous-Saint-Paul Cave connected to the upper gallery through vertical pits that are mostly filled with sediment. Only the connection in the entrance zone is visible in the figure.

laboratories. The analyses were performed by MC-ICP-MS but with different instruments in the individual laboratories.

At Xi'An Jiaotong University, China, U and Th were co-precipitated using a Fe solution and subsequently extracted using an anion exchange resin (BioRad AG 1-X8) to extract Th and U, respectively. The final solution was analyzed on a Thermo Fisher Scientific Neptune Plus MC-ICP-MS. The entire procedure was carried out at the Institute of Global Environmental Change at Xi'an Jiaotong University (China) and followed established protocols (e.g., Cheng et al., 2020).

At the University of Melbourne, Australia, sample preparation and chemical separation of U and Th and MC-ICP-MS measurements followed established protocols (Hellstrom, 2003). The equilibrated and spiked solution was loaded onto an ion exchange column containing Eichrom TRU and prefilter resin to discard the calcite matrix and finally elute U and Th. The U–Th fractions were analyzed on a Nu Instruments Plasma MC-ICP-MS at the University of Melbourne (e.g., Weij et al., 2024).

At the Max Planck Institute for Chemistry (MPIC) in Mainz, Germany, U and Th were separated from the spiked sample solution using ion exchange column chemistry (Yang et al., 2015) and analyzed using a Nu Instruments Plasma MC-ICP-MS (Obert et al., 2016).

At the Institute for Geosciences, Johannes Gutenberg University (JGU) in Mainz, Germany, samples were passed through ion exchange columns filled with 1.5 mL of Bio-Rad AG 1-X8 anion exchange resin to separate U and Th. Mass spectrometric analyses of U and Th (cf. Obert et al., 2016) were conducted using a Thermo Fisher Scientific Neptune Plus MC-ICP-MS.

All activity ratios and ages were calculated using the half-lives reported by Cheng et al. (2013) and corrected for detrital contamination assuming a $^{232}Th/^{238}U$ weight ratio of 3.8

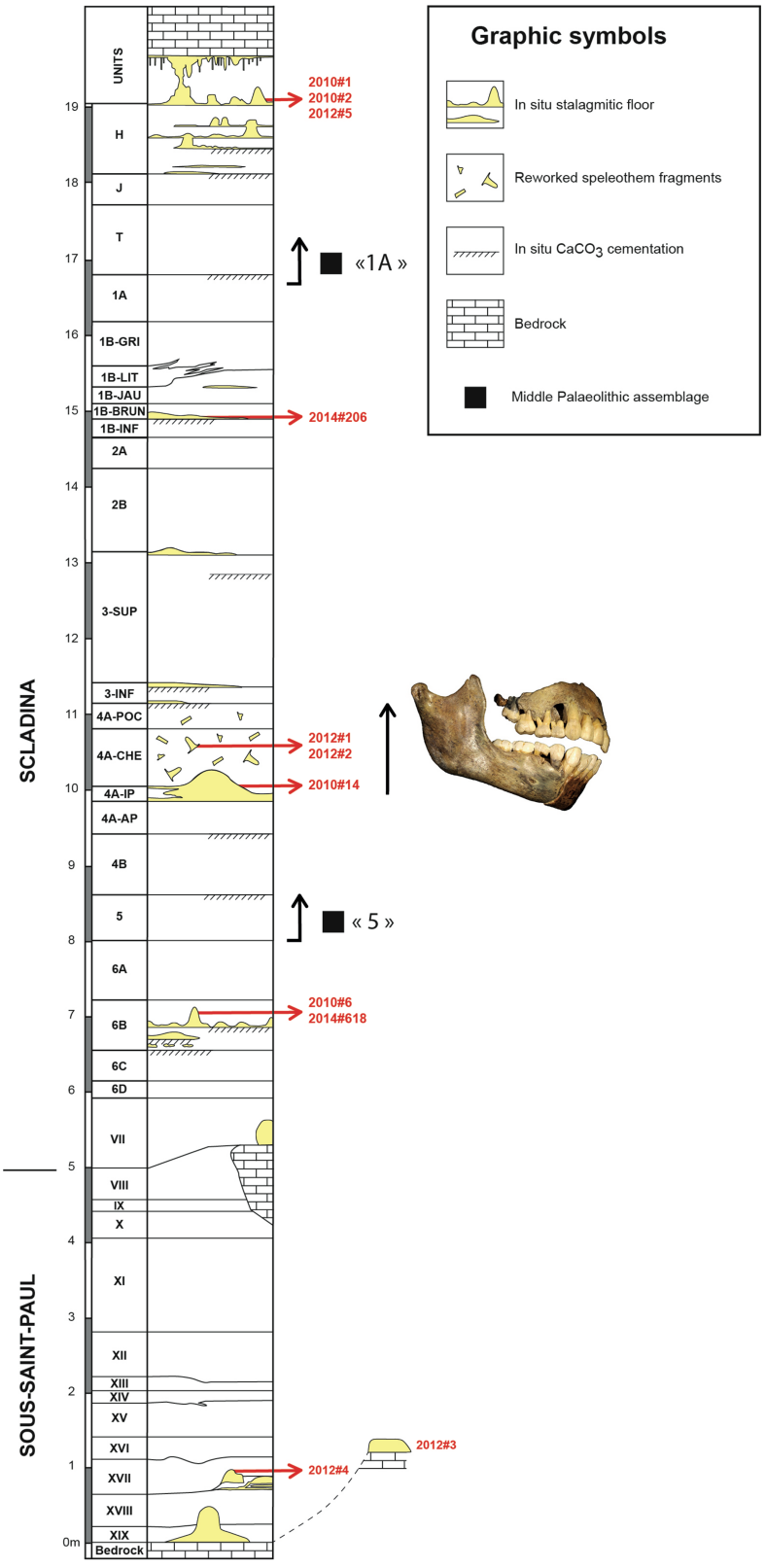

Figure 3. Schematic stratigraphic column of the combined Scladina Cave and Sous-Saint-Paul Cave sedimentary sequence. Speleothem occurrences are indicated in yellow coloring. The vertical scale bar is in meters. The position of the samples that were dated in this study is indicated by the red arrows. The photograph is placed to indicate the position that the Neanderthal mandible and teeth were found in unit 4A.

for the detritus and ^{230}Th, ^{234}U, and ^{238}U in secular equilibrium (Wedepohl, 1995). To account for the uncertainty in the correction, we assumed an uncertainty of 50 %, which was fully propagated to the corrected activity ratios and ages. All uncertainties are reported at the 2σ level.

2.3 Stable isotope analysis of $CaCO_3$

Samples were analyzed on a Thermo Fisher Scientific Delta-V mass spectrometer at MPIC Mainz equipped with a Gasbench II preparation device. About 8–50 µg of $CaCO_3$ sample, placed in a He-filled 12 mL exetainer vial, was digested in >99 % H_3PO_4. Subsequently, the CO_2–He gas mixture was transported to the Gasbench in 5.0-grade helium carrier gas. In the Gasbench, water vapor and various gaseous compounds were separated from the He–CO_2 mixture prior to sending it to the mass spectrometer for isotope analysis and reported as $CaCO_3\delta^{13}C$ ($\delta^{13}C_{cc}$) and $CaCO_3\delta^{18}O$ ($\delta^{18}O_{cc}$) on the "Vienna Peedee Belemnite" (VPDB) scale.

The In-house $CaCO_3$ standard VICS (having a $\delta^{13}C$ value of 1.45 ‰ VPDB and a $\delta^{18}O$ value of -5.44 ‰ VPDB) was analyzed with each run of samples. $CaCO_3$ standard weights of standards are chosen so that they span the entire range of sample weights of the samples. After correction of isotope effects related to sample size, the reproducibility of the standards is typically better than 0.1 ‰ (1 SD) for $\delta^{18}O$ and 0.1 ‰ (1 SD) for $\delta^{13}C$.

2.4 Stable isotope analysis of dripwater

A single dripwater sample from Scladina Cave taken on 5 July 2010 was analyzed by use of a Thermo Fisher Scientific TC-EA pyrolysis furnace coupled to a Delta XP mass spectrometer at Vrije Universiteit Amsterdam (VU). Analytical precision (1 SD) of four in-house water standards (eight repetitive analyses for each) in the sample series that contained this sample did not exceed 0.2 ‰ for $\delta^{18}O$ and 1.0 ‰ for $\delta^{2}H$. Triplicate analysis of the sample itself resulted in a 1 SD precision smaller than that of the standard water reproducibility. Isotope data of the dripwater sample is reported on the "Vienna Standard Mean Ocean Water" (VSMOW) scale.

2.5 Fluid-inclusion isotope analysis

Fluid-inclusion isotope analyses were performed on discrete $\sim$0.5–1.0 g chips of speleothem calcite, cut from the speleothem slabs using a Dremel microdrill with diamond-lined rotary drill blade. These samples were crushed under a controlled atmosphere in a crushing cell attached to a Picarro L2140*i* water isotope analyzer at the Max Planck Institute for Chemistry in Mainz, Germany. The resulting hydrogen and oxygen isotope values of fluid-inclusion water ($\delta^{2}H_{fi}$ and $\delta^{18}O_{fi}$, respectively) are reported on the VSMOW scale. Typical 1 SD precisions for this technique, based on standard water injections in this system, are better than 0.3 ‰ for $\delta^{18}O_{fi}$ values and 1.0 ‰ for $\delta^{2}H_{fi}$ values (De Graaf et al., 2020).

2.6 Laser ablation trace element analysis

Trace element concentrations were measured by laser ablation ICP-MS at the MPIC following the procedure of Jochum et al. (2012), with a high-resolution sector field ICP-MS ThermoElement2, interfaced with a New Wave UP-213 Nd:YAG laser ablation system. The silicate glass NIST SRM 612 was analyzed for external calibration of the trace element analyses. Data are reported in parts per million (ppm) notation.

3 Results

3.1 Cave site and regional climate

The mean annual surface temperature in the nearby town of Andenne is $\sim$ 10.4 °C, and average monthly temperatures typically range between 3 and 18 °C (KMI, 2024). Cave temperature monitoring from July 2010 until July 2011 showed an annual cycle between 8 and 13 °C, with an average annual value of 10.5 °C, which is dampened in seasonality but very close to the mean annual surface temperature of the region. Based on accounts of the archeological staff on site, drip rates in the cave are variable, depending on rainfall amounts above the cave. This likely relates to the small hydrological catchment area of Scladina Cave (see Fig. 1). Relative humidity measurements in the cave taken at different points in time typically were close to 100 %.

3.2 Diagenetic screening of speleothem samples

The thinner speleothem layers, present in the cave sediments, commonly appear significantly altered, which is macroscopically evidenced by yellow and brownish discoloration and sometimes even loss of the original "brittle" nature of the calcite. Such altered samples have become much softer than pristine speleothem calcite from this site. In contrast, the more prominent speleothem layers, particularly when developed in stalagmite morphology, appear to be much better preserved visually. Stalagmites growing from the top of unit H (specimens 2010#1, 2010#2, and 2012#5) appear well preserved overall, presumably because they represent the only material that has not been covered by siliciclastic sediments.

Speleothems collected from under unit H have all been buried in siliciclastic sediments. These speleothems often show discoloration on the outer surface that looks much like those of the poorly preserved material from the thinner layers. For some specimens, like 2014#618, the discoloration appears on the inside of the speleothem as well but generally closer to the surface that had been exposed to the siliciclastic sediment. In all stalagmite material we took subsamples from near the growth axis, avoiding visible discoloration, and

targeting areas that showed clear lamination that we interpreted to be the original calcite fabric. Thin-section observations from several of these samples reveal columnar fabrics (Fig. 4), which are generally taken to represent unaltered speleothem calcite (Frisia et al., 2000), suggesting that this sampling strategy indeed selects the well-preserved material. One thin section of a sample that seemed less well preserved (2012#6) shows fine microsparite (Fig. 4), which is considered to point towards diagenetic recrystallization. That sample was removed from the dataset before further analysis.

Two flow stones from the Sous-Saint-Paul Cave (2012#3 and 2012#4) were sampled along the central axis of the sample we took and show columnar calcite fabrics (Fig. 4).

The effect of diagenetic alteration on speleothem material that was buried in siliciclastic sediments in the cave was geochemically characterized in a laser ablation ICP-MS transect measured at high spatial resolution from the visually well-preserved core of stalagmite 2014#618 (unit 6B) to its diagenetically altered outer surface (Fig. 5). The transect is 42 mm long in total. Whitish and yellowish discoloration, black irregular laminae, and loss of visible lamination and transparency towards the more altered zone near the outer surface of the speleothem suggest diagenetic alteration upon macroscopic inspection. Calcite fabric at the growth axis lacks these features and looks macroscopically unaltered.

Clearly shown in the trace element data is that ^{238}U and ^{232}Th have high concentrations at the outer surface of the stalagmite, which has been in direct contact with the sediment in which it was buried. The ^{238}U shows a gradient of decreasing values towards the core of the speleothem, reaching stable $\sim$0.1 ppm concentrations in the central growth axis of the speleothem, which represents the $CaCO_3$ material that appears unaltered at visual inspection. This gradient is much sharper for ^{232}Th, which shows markedly increased values only at the outer surface of the stalagmite.

Elements like strontium and phosphorus show patterns very comparable to that of U^{238}. In contrast, the Mn distribution does not compare well to that of ^{238}U or ^{232}Th.

Please note that single scattered data points towards higher values, best visible in the ^{88}Sr and ^{232}Th traces in Fig. 5, are considered to be analytical artifacts (outliers) occurring during laser ablation.

3.3 U–Th ages

The results of U–Th dating are presented in Table 1 and Fig. 6. All ages are reported as ka Before Present (BP), where the Present is defined as the year 1950 CE. The speleothems from unit H all yield Holocene ages, which generally confirms previously published U–Th ages of this unit (Gewelt et al., 1992). The stratigraphically oldest sample from the base of stalagmite 2012#5 from that speleothem complex reaches 8.9 ka, and the ages of the composite record of stalagmites on top of unit H seem to suggest near-continuous speleothem growth until the present day.

Stalagmite 2014#206 from layer 1B-BK (unit 1B-BRUN) produced four ages (Table 1). Two of which, at the base of the stalagmite, indicate growth in MIS-5a, and another two higher up in the stalagmite correspond to MIS-3 (Fig. 6). Comparatively little stalagmite growth thickness between these two age clusters may suggest reduced or no growth in MIS-4.

Unit 4A stalagmites yield consistent ages that all fit in MIS-5e, which is the warmest stage of MIS-5 (Table 1; Fig. 6). The oldest ages we captured for unit 4A are from 121 ka. The youngest age for the two unit-4A stalagmites analyzed is 116 ka.

Two stalagmites from flowstone levels in stratigraphic unit 6B yield ages at 197 ka for specimen 2014#618 and ages from 142 to 174 ka for specimen 2010#6. The older ages can be attributed to the warm period MIS-7a, which fits the general pattern that in Scladina Cave speleothems grew predominantly during interglacials. Interestingly, the younger age range of specimen 2010#6 places it in MIS-6, which is a glacial period.

The next speleothem level further down in the Scladina Cave stratigraphy is in fact situated in the underlying Sous-Saint-Paul Cave, in unit XVII, which is connected to Scladina Cave by an open vertical shaft near the entrance of the cave. For the sub-samples taken from flowstone sample 2012#4, we have consistent ages of 300–311 ka at $\pm$9 ka 2σ uncertainties, suggesting the flowstone formed under interglacial conditions in MIS-9 (Fig. 6; Table 1).

The lowest speleothem level encountered in the Sous-Saint-Paul Cave (2012#3) is again a flowstone layer, related to unit XIX. For this layer the ages plot between 363 and 536 ka (Table 1) as measured in three labs and roughly spanning the time period between MIS-14 and MIS-10. The ages are partly inversed, which is perhaps not surprising in view of the high and variable dating uncertainties (from 105 to 14 ka at 2σ level) in a time interval that is so close to the limit of what can still be dated with the U–Th technique. In any case, the ages of Sous-Saint-Paul Cave suggest that its sedimentary infill predates that of Scladina Cave.

3.4 Fluid-inclusion stable isotope data

For all specimens studied we performed isotope analysis of fluid-inclusion water on multiple subsamples. The isotope composition of fluid-inclusion water in speleothem calcite (δ^2H_{fi} and $\delta^{18}O_{fi}$) is considered to represent that of the dripwater in the cave at the time of speleothem growth, which in turn is a direct proxy for the isotope composition of (paleo)rainfall recharging the cave aquifer (Dennis et al., 2001; Van Breukelen et al., 2008). The oldest specimen, 2012#3, contained too little fluid-inclusion water for analysis. Fluid-inclusion isotope values from most other speleothems, presented in Table 2 and Fig. 7, fall on a trend with part of the samples plotting around an endmember close to the Global Meteoric Water Line (GMWL).

Table 1. Results of the ^{230}Th/U dating of the Scladina samples (the ages are reported in ka) DFT stands for distance from top..

Sample	DFT [mm]	Lab	^{232}Th [ng g^{-1}]	Uncertainty	^{238}U [mg g^{-1}]	Uncertainty	(^{234}U/^{238}U)	Uncertainty	(^{230}Th/^{238}U)	Uncertainty	(^{230}Th/^{232}Th)	Uncertainty	Uncorrected age [ka]	Uncertainty	Corrected age [ka]	Uncertainty [ka]
2010#1	22	Melbourne	0.427	0.038	0.173	0.013	1.0417	0.0036	0.00765	0.00055	9.72	0.82	0.740	0.057	0.673	0.066
2010#1	102	Melbourne	0.238	0.023	0.209	0.016	1.0414	0.0029	0.00986	0.00060	27.2	2.2	0.974	0.063	0.943	0.065
2010#1	152	Melbourne	0.332	0.032	0.211	0.016	1.0414	0.0037	0.01127	0.00091	22.4	2.3	1.122	0.097	1.080	0.097
2010#1	256	Melbourne	0.240	0.025	0.190	0.014	1.0516	0.0030	0.01521	0.00045	37.8	2.2	1.524	0.048	1.491	0.051
2010#1	330	Melbourne	2.23	0.18	0.220	0.017	1.0542	0.0031	0.02410	0.00073	7.47	0.27	2.458	0.078	2.19	0.15
2010#1	418	Melbourne	0.782	0.069	0.214	0.016	1.0512	0.0038	0.0293	0.0013	25.2	1.4	3.02	0.13	2.92	0.15
2010#2	80	Melbourne	2.18	0.19	0.211	0.016	1.0422	0.0032	0.01310	0.00065	3.99	0.24	1.316	0.070	1.04	0.15
2010#2	170	Melbourne	0.872	0.076	0.212	0.016	1.0480	0.0037	0.01536	0.00088	11.71	0.81	1.546	0.092	1.44	0.11
2010#2	415	Melbourne	2.15	0.18	0.223	0.017	1.0476	0.0037	0.02999	0.00096	9.74	0.40	3.10	0.10	2.85	0.16
2010#2	530	Melbourne	17.3	1.5	0.187	0.014	1.0513	0.0090	0.0669	0.0044	2.27	0.17	7.11	0.48	4.6	1.3
2012#5	0	Melbourne	1.26	0.10	0.196	0.015	1.0495	0.0039	0.03646	0.00049	17.84	0.32	3.788	0.055	3.62	0.10
2012#5	376	Melbourne	1.88	0.15	0.187	0.014	1.0400	0.0034	0.06576	0.00059	20.53	0.29	7.053	0.068	6.78	0.15
2012#5	740	Melbourne	40.7	3.2	0.203	0.015	1.0172	0.0035	0.1202	0.0017	1.878	0.033	13.64	0.22	8.0	2.9
2012#5	740	Mainz JGU	1.2056	0.0076	0.1911	0.0011	1.0358	0.0005	0.08226	0.00037	39.86	0.19	8.964	0.042	8.789	0.096
2014#206	20	Xi'An	36.61	0.74	0.25621	0.00074	1.1042	0.0026	0.4608	0.0018	9.86	0.20	58.25	0.35	54.5	1.8
2014#206	40	Xi'An	11.91	0.24	0.21763	0.00031	1.3464	0.0019	0.5429	0.0013	30.33	0.61	54.84	0.20	53.72	0.50
2014#206	75	Xi'An	6.67	0.13	0.29772	0.00057	1.0895	0.0018	0.5415	0.0014	73.8	1.5	74.01	0.32	73.42	0.42
2014#206	85	Xi'An	8.91	0.18	0.23302	0.00037	1.0737	0.0017	0.5619	0.0012	44.93	0.90	79.86	0.33	78.86	0.57
2010#14	25	Melbourne	8.09	0.65	0.237	0.018	1.0769	0.0041	0.7199	0.0088	66.2	1.1	118.0	2.7	117.2	2.7
2010#14	97	Melbourne	0.833	0.075	0.254	0.019	1.1059	0.0047	0.7351	0.0066	704	17	116.1	2.0	116.0	2.1
2010#14	150	Melbourne	3.15	0.26	0.326	0.025	1.1301	0.0044	0.7586	0.0077	246.5	4.5	117.5	2.2	117.3	2.3
2012#2	40	Melbourne	0.298	0.025	0.191	0.014	1.0741	0.0030	0.7117	0.0030	1433	17	116.2	1.1	116.2	1.1
2012#2	255	Melbourne	0.375	0.030	0.208	0.016	1.0589	0.0021	0.7079	0.0029	1228	10	118.50	0.98	118.5	1.0
2012#2	310	Melbourne	7.81	0.64	0.198	0.015	1.0597	0.0021	0.7124	0.0027	56.58	0.59	119.70	0.93	118.7	1.0
2012#2	410	Melbourne	0.590	0.050	0.186	0.014	1.0609	0.0028	0.7165	0.0047	707	11	120.6	1.6	120.6	1.6
2012#1	2	Mainz MPIC	11.66	0.12	0.2160	0.0014	1.0604	0.0016	0.7215	0.0044	40.84	0.42	122.3	1.4	120.8	1.6
2012#1	84	Mainz MPIC	2.282	0.024	0.2332	0.0016	1.0709	0.0016	0.7222	0.0036	225.6	2.1	120.0	1.1	119.8	1.2
2012#1	172	Mainz MPIC	3.308	0.033	0.1810	0.0012	1.0656	0.0020	0.7199	0.0038	120.4	1.1	120.6	1.2	120.1	1.3
2012#1	244	Mainz MPIC	7.831	0.078	0.1895	0.0012	1.0768	0.0017	0.7279	0.0035	53.85	0.49	120.4	1.1	119.3	1.2
2010#6	35	Mainz JGU	4.237	0.030	0.2550	0.0016	1.09156	0.00042	0.8087	0.0029	148.79	0.67	142.7	1.0	142.2	1.1
2010#6	48	Melbourne	11.35	0.92	0.256	0.019	1.0736	0.0054	0.8624	0.0083	61.02	0.96	171.2	4.6	170.1	4.6
2010#6	70	Mainz JGU	1.2052	0.0085	0.2877	0.0018	1.07447	0.00033	0.8694	0.0033	634.3	3.1	174.0	1.6	173.9	1.6
2014#618 SV12	40	Xi'An	3.289	0.066	0.25767	0.00029	1.0492	0.0012	0.8857	0.0013	212.0	4.3	196.5	1.1	196.1	1.1
2014#618 SV11	180	Xi'An	7.37	0.15	0.23568	0.00025	1.0549	0.0013	0.8934	0.0013	87.3	1.8	197.6	1.1	196.7	1.2
2014#618-3	80	Mainz MPIC	0.3955	0.0055	0.2337	0.0016	1.0545	0.0026	0.8919	0.0058	1610	22	196.9	3.9	196.8	3.9
2012#4	20	Melbourne	0.703	0.059	0.184	0.014	1.1094	0.0026	1.0734	0.0046	883	11	303.7	+8.2–7.7	303.7	+8.4–7.6
2012#4	48	Mainz MPIC	1.156	0.012	0.1475	0.0010	1.1069	0.0020	1.0679	0.0059	416.6	4.1	300.4	+9.4–8.6	300.2	8.8
2012#4	48	Melbourne	5.73	0.47	0.147	0.011	1.1043	0.0023	1.0728	0.0052	86.50	0.95	312.0	9.2	311.1	+9.4–8.4
2012#4	84	Melbourne	9.49	0.81	0.192	0.014	1.1074	0.0029	1.0709	0.0052	67.8	1.0	303.6	+9.3–8.6	302.5	+9.4–8.6
2012#3	15	Melbourne	0.157	0.013	0.276	0.021	1.0849	0.0024	1.0949	0.0057	6040	83	429	+32–25	429	+33–26
2012#3	15	Mainz MPIC	0.0852	0.0018	0.2941	0.0020	1.0838	0.0023	1.1026	0.0100	11630	260	477	+101–55	477	+105–55
2012#3	35	Melbourne	0.213	0.018	0.240	0.018	1.0881	0.0034	1.0998	0.0049	3895	59	431	+35–27	431	+34–26
2012#3	50	Melbourne	0.141	0.012	0.381	0.029	1.0907	0.0020	1.1031	0.0035	9379	100	430	+21–17	430	+22–18
2012#3	50	Mainz MPIC	0.0722	0.0016	0.5491	0.0036	1.0982	0.0027	1.092	0.011	25370	580	363	+29–24	363	+31–23
2012#3 SV10	10	Xi'An	0.603	0.012	0.33958	0.00039	1.0822	0.0012	1.1001	0.0016	1894	38	475	+16–14	475	+16–14
2012#3 SV9	45	Xi'An	0.1411	0.0029	0.29206	0.00032	1.0876	0.0012	1.1150	0.0017	7060	140	536	+29–23	536	+30–23

https://doi.org/10.5194/cp-20-2741-2024 Clim. Past, 20, 2741–2758, 2024

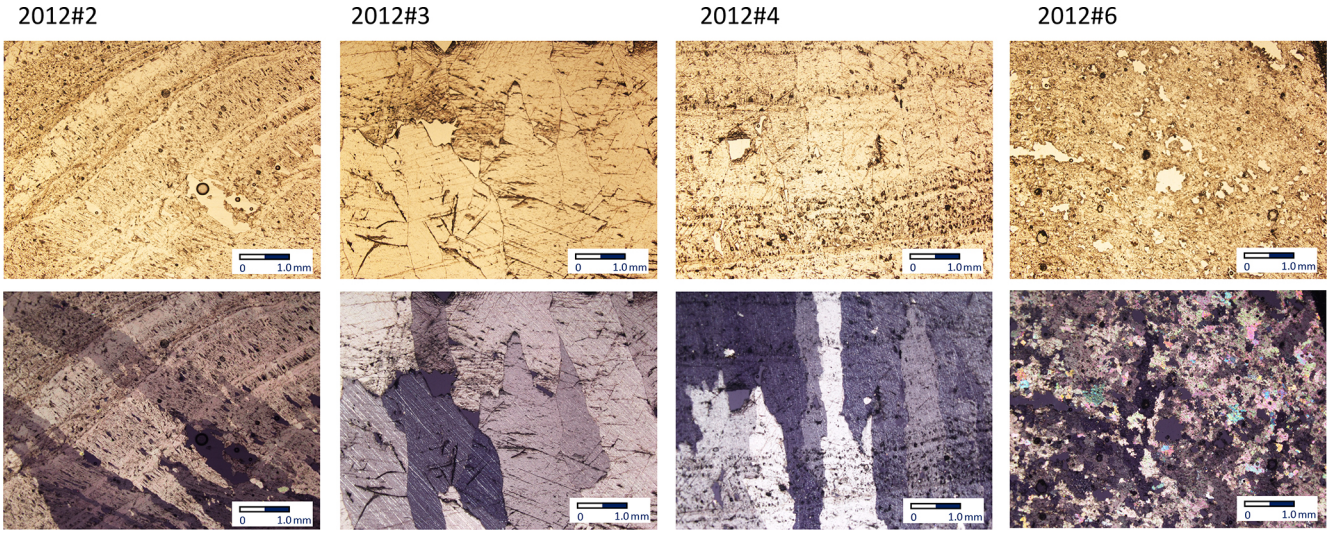

Figure 4. Some representative thin-section images of the speleothem material studied. The top row consists of plain-light (PL) images, with the growth direction generally being upward. The bottom row shows the same pictures in cross-polarized light (CPL). Specimens 2012#2 and 2012#4 show micro-scale growth banding of speleothem calcite in PL and cross-cutting columnar crystallographic fabric visible in CPL, which we interpret to reflect well-preserved speleothem calcite. Fluid inclusions in these images are shown as small black dots that generally line up along the growth bands. The images of specimen 2012#3 show no growth banding, relatively coarse crystals that are elongated in the growth direction, and a conspicuous scarcity of fluid inclusions. The images of specimen 2012#6 show a lack of growth banding and very small equidimensional crystals that we interpret to indicate diagenetic alteration of speleothem calcite. That specimen was discarded and has not been further analyzed in this study.

Part of the data trend away from the GMWL at a relatively low angle towards higher δ^2H_{fi} and $\delta^{18}O_{fi}$ values (Fig. 7). This trend seems to occur in data from all studied time intervals with one clear exception. This exception is specimen 2012#4, dated at MIS-9 age, which displays the lowest δ^2H_{fi} and $\delta^{18}O_{fi}$ data of all material analyzed and plots in a tightly constrained field close to the GMWL (Fig. 7).

The fluid-inclusion isotope data that plot near the GMWL have isotope values close to the annually averaged isotope composition of modern regional rainwater (δ^2H_p and $\delta^{18}O_p$) of $-47.3\,‰$ and $-6.8\,‰$ (VSMOW) for δ^2H and $\delta^{18}O$, respectively. Rainfall data are provided by the Global Network of Isotopes in Precipitation (IAEA/WMO, 2023) database for the Liège weather station (for the years 1966–1970). A single dripwater sample from Scladina Cave (taken on 5 July 2010) gave a δ^2H value of $-42.4\,‰$ and a $\delta^{18}O$ value of $-6.5\,‰$, which is also close to the weighted-average rainfall isotope values for Liège, as documented in the Global Network of Isotopes in Precipitation database.

4 Discussion

4.1 Diagenetic screening of the samples

While there is no doubt that diagenesis has at least partly altered the Scladina Cave speleothems, we have made several observations indicating that diagenesis is not pervasive, and in the samples we selected for U–Th analysis we successfully avoided diagenetically altered parts of the speleothems. The laser ablation ICP-MS trace element patterns (Fig. 5) in particular suggest significant diagenetic alteration on the stalagmite outer surface, while the calcite in the growth axis shows trace element concentrations that fit unaltered speleothem calcite. The different gradients of ^{238}U and ^{232}Th from the diagenetic surface towards the unaltered growth axis are interpreted to reflect the contrasting solution chemistry of U and Th. U can move in dissolved form with diagenetic fluids into the speleothem, while the less soluble Th, stays behind in particulate or colloidal state on the outside. Elements like strontium, which are also readily mobile in solution, show very comparable concentration trends to uranium, suggesting that, once buried in detrital cave sediments, a dissolution–reprecipitation diagenetic front penetrated into the speleothems from the surface inwards, altering trace element patterns.

Diagenetic alteration of speleothem calcite is described in several earlier studies, and different diagenetic processes have been suggested. Commonly observed is the post-depositional transition from aragonite to calcite fabrics (Frisia, 2015, and references therein), which is a process we do not believe to be of significance for the present study, as we find no evidence for aragonite mineralogy in our material. Another process is redissolution of speleothem material due to changing dripwater chemistry, which may lead to recrystallization along the stalagmite growth axis (Scholz et al., 2014). Further, neomorphism, or "cryptic" diagenesis

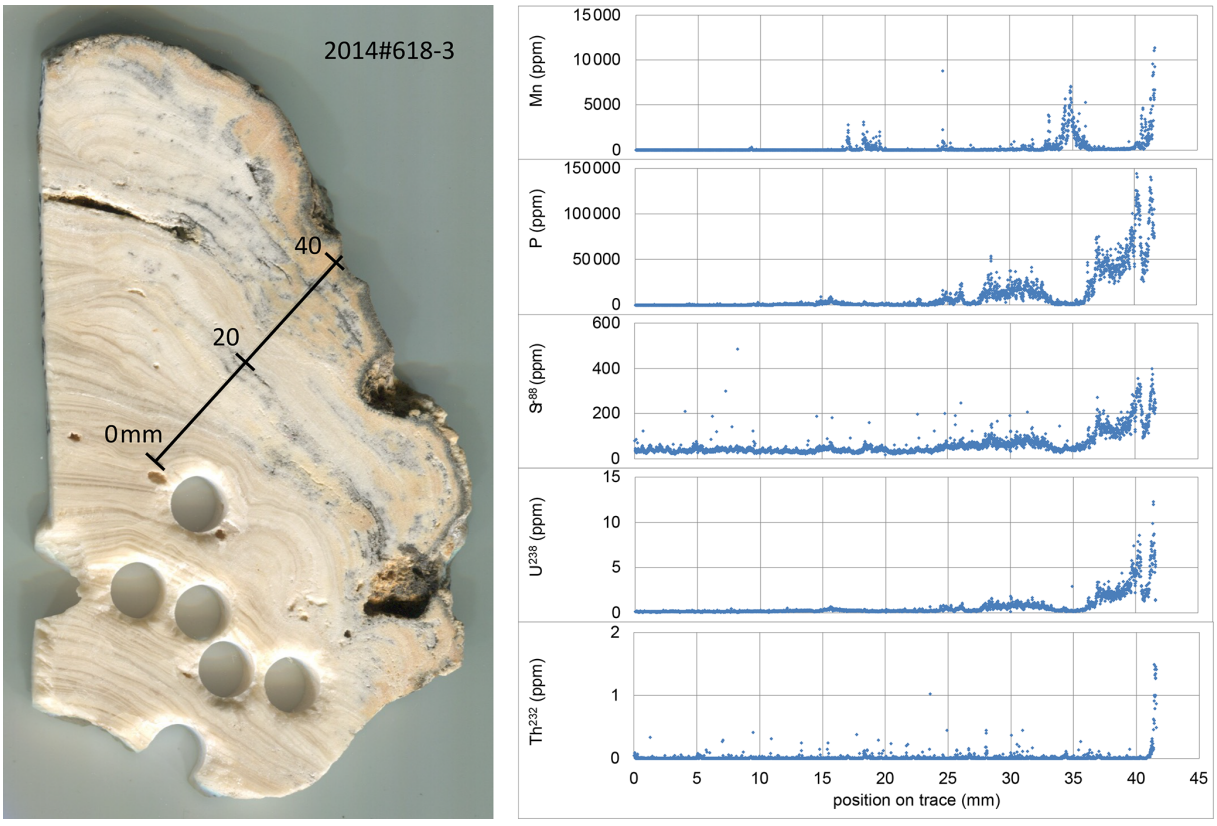

Figure 5. Stalagmite sample 2014#618 shows clear discoloration towards the right side of the stalagmite that was exposed to the sediment in which it was buried. Laser ablation trace element analysis along the 42 mm long transect shown in the picture demonstrates that manganese is associated with the blackish layers that occur in the exterior portions of the stalagmite. It is also clear that significant enrichment of U and Th occurs at the surface of the stalagmite that has been in contact with the sediment in which it was covered. Uranium declines gradually from the outer surface towards the center of the stalagmite. Sr shows a similar pattern to U. The Th content of the entire trace can be considered very low, with the exception of the increased Th concentration on the outer surface. Circular holes in the basal part of the sample are samples taken for earlier investigations unrelated to the present study.

has been reported for stalagmites (Bajo et al., 2016; Frisia, 2015) which is often seen as fine-scale infiltration of water in speleothems accompanied by thin-film dissolution – re-precipitation reactions capable of affecting the geochemical composition of speleothems, without clearly visible changes to the texture of the calcite. The latter process has been suggested to be able to affect U–Th ages (Bajo et al., 2016).

The diagenetic patterns that we observe in the trace element data seems to be in line with such neomorphic processes. Also, the less commonly observed elevated phosphorous content, which lines up well with a diagenetic increase in U and Sr, likely results from mobilization of bat guano phosphate present in the detrital sediment matrix, and subsequent diagenetic precipitation in the speleothem calcite fabric (Audra et al., 2021).

For the present study, the most important observation is that well before the transect reaches the growth axis of the speleothem, the trace element concentrations stabilize at values that are typical of well-preserved speleothem calcite. It therefore appears that the speleothem calcite we selected for U–Th analysis is sufficiently well preserved to yield good radiometric ages.

One more observation that follows from the trace element data is that the black laminae, occurring in some of the specimens studied, contain manganese. These manganese enrichments do not line up with the diagenetic patterns in Sr, U, and P. If these Mn enrichments are diagenetic, it appears that they are not formed by the same diagenetic process. In any case, we stayed away from these dark laminae when sampling for U–Th analysis.

This careful diagenetic screening of speleothem samples has led to what appears to be a relatively consistent U–Th chronology of the Scladina speleothem sequence. When properly applying ^{232}Th corrections and considering the analytical uncertainties that result from that, no age reversals are present in the dataset, with the exception of the samples from the oldest flowstone level 2012#3, which are very close to the dating limit of the U–Th technique. Where different specimens from a single stalagmite horizon were analyzed, the re-

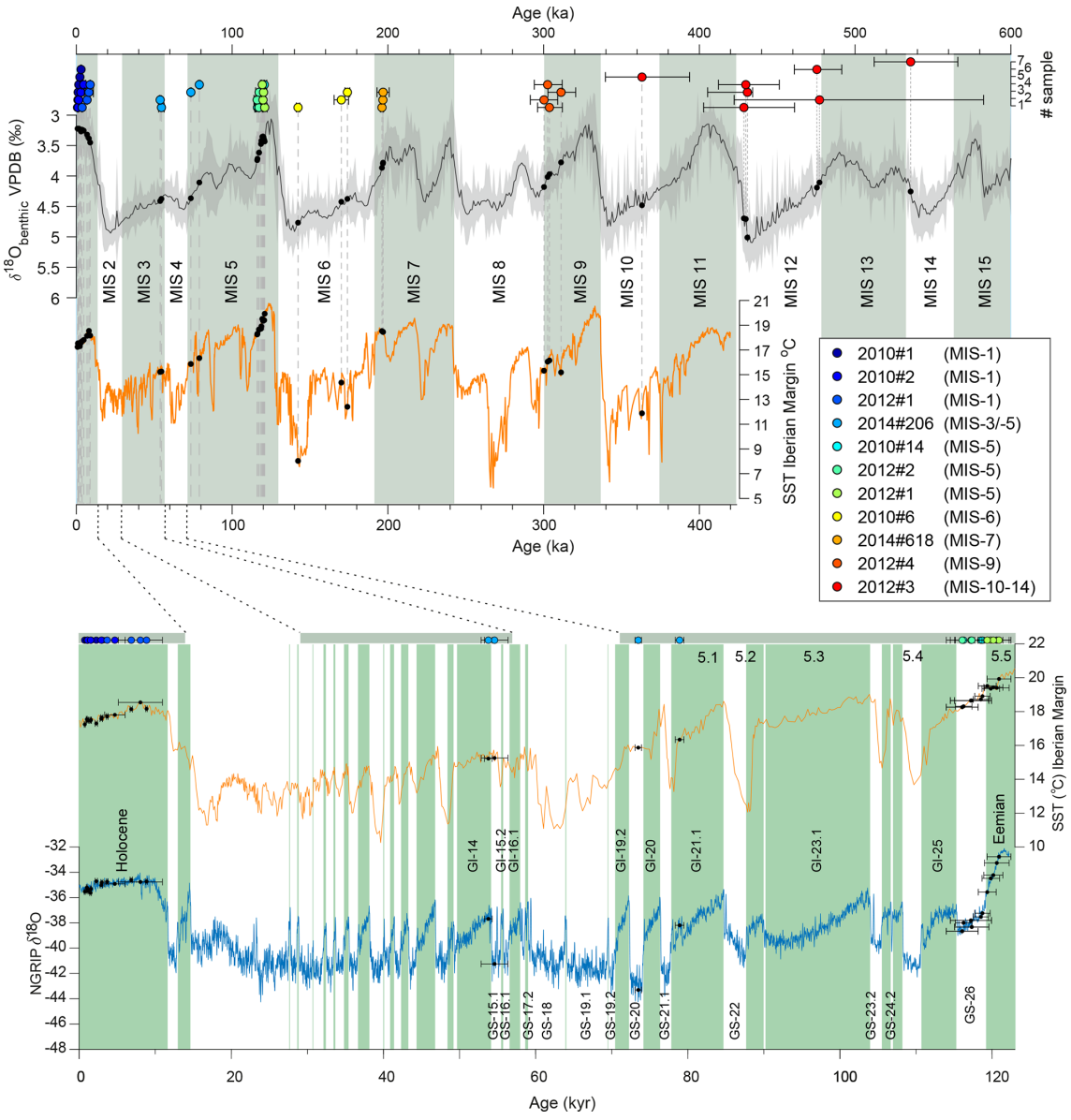

Figure 6. The U–Th ages of the individual speleothems that were obtained in this study are plotted as colored dots with their 2σ-uncertainty limits and are projected onto global and regional climate proxy records. The global benthic $\delta^{18}O$ probabilistic stack (Ahn et al., 2017), with the mean and 95 % confidence interval given as a solid black line and gray area, respectively. This global benthic $\delta^{18}O$ stack provides the glacial–interglacial variability, whereby the glacial and interglacial (gray bars) marine isotope stages are defined by Lisiecki and Raymo (2005). The orange line indicates the Uk'37 sea surface temperature (SST) record from marine sediment core MD01-2443 off the Iberian Margin (Martrat et al., 2007). The high-resolution $\delta^{18}O$ record of the North Greenland Ice Core Project (NGRIP) site is plotted as a blue line together with the Greenland stadials (GSs) and interstadials (GIs: green bars) (Rasmussen et al., 2014; Seierstad et al., 2014).

sulting ages appear generally consistent, and this is also the case between the different labs where the dating took place.

4.2 Fluid-inclusion isotope ratios

In "low-water–rock-ratio" systems like speleothem calcite and its fluid inclusions, diagenetic alteration is expected to impact the fluid-inclusion isotope composition more readily than it will impact the calcite (Uemura et al., 2020).

Still, about half of fluid-inclusion isotope data in Fig. 7 plots close to the GMWL, which suggests that these isotope data still represent the original rainwater values. This is corroborated by the relatively good comparison of these fluid-inclusion isotope data to modern dripwater and rainwater isotope values from the area. The observation that another subset of the fluid inclusions trend away from the GMWL (Fig. 7) resembles a case of diffusive water loss from

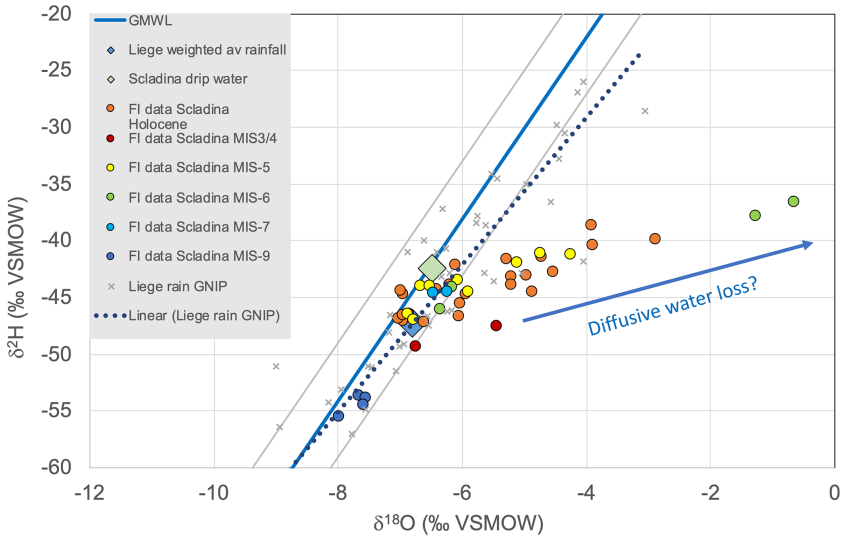

Figure 7. Fluid-inclusion isotope data of Scladina speleothems shown as round plot symbols. GNIP rainfall isotope data for Liège in the time period between 1966 and 1970 are indicated as gray crosses. The GMWL is shown as a solid blue line, and the local (Liège) meteoric water line (MWL) is shown as a dotted blue line. Parallel gray lines indicate the GMWL+5 to GMWL-5 envelope around the GMWL. The annually averaged rainwater isotope value and the dripwater isotope composition in the cave are shown as diamonds.

speleothem calcite, reported as being the result of an analytical artifact in a recent study by Fernandez et al. (2023). Fernandez and co-workers describe how sample heating prior to isotope analysis in fluid-inclusion isotope instrumentation can lead to partial water loss from fluid inclusions because the host mineral loses sealing capacity under higher temperatures. Such partial water loss leads to isotope fractionation of the remaining water. While in the study by Fernandez et al. (2023) diagenesis did not play a role, we postulate that diagenetic alteration may have contributed to the weakening of the fluid-inclusion sealing capacity in the case of Scladina Cave, leading to isotope fractionation very similar to what Fernandez et al. (2023) describe. Thus, the fluid-inclusion isotope data of diagenetically compromised samples are more likely to plot away from the GMWL. This seems to be supported by the observation that two samples taken from the most altered parts of stalagmite 2014#618-3 (Table 2) already lost so much of their water in the warm-up stage (presumably because of diagenetic weakening of fluid-inclusion sealing) that they could no longer be analyzed.

We next combined the oxygen isotope composition of the fluid inclusions ($\delta^{18}O_{fi}$) with that of the corresponding host calcite ($\delta^{18}O_c$) to calculate past cave temperatures based on the assumption of (1) isotope equilibrium during formation and (2) the absence of post-depositional alteration of fluid-inclusion water or calcite (Table 2). Based on a widely accepted calculation specifically made for speleothems (Tremaine et al., 2011), these data show that fluid-inclusion isotope values plotting further away from the GMWL lead to unrealistically high temperatures (Fig. B1), which supports the idea that these fluid-inclusion isotope values indeed were no longer original when they were measured. Most of the data plotting close to the GMWL, however, result in paleotemperatures in the range of the modern (interglacial) cave temperatures, suggesting, in good agreement with the observations by Fernandez et al. (2023), that these fluid-inclusion and calcite isotope values are essentially unaltered and provide what we interpret to be the original rainwater isotope values during formation of the speleothems.

4.3 Paleoclimatological backdrop of speleothem growth in Scladina Cave

Based on the robust age framework for the horizons of speleothem growth in Scladina Cave it is now possible to consider the paleoclimatological backdrop of speleothem growth at this site in more detail than previously possible. Alignment of the Scladina speleothem ages along the late Quaternary Probabilistic Benthic Stack (Ahn et al., 2017) confirms that speleothem growth in Scladina Cave generally took place during Interglacial periods. (Fig. 6). During Glacial periods, sedimentation in Scladina Cave was dominated by siliciclastic influx (Pirson et al., 2014b).

Ages for the oldest speleothem (flowstone) material in this record have higher age uncertainties, and can therewith not be tied to a single interglacial period. All we can say is that growth occurred in the time period from MIS-10 to MIS-14 based on the U–Th data we collected for these older samples.

Finally, two speleothems have ages that suggest deposition in non-interglacial conditions. Stalagmite 2010#6 has U–Th ages ranging from 174 to 142 ka, which corresponds to glacial period MIS-6, and stalagmite 2014#206 has ages

Table 2. Stable isotope data of Scladina Cave fluid-inclusion water samples and one dripwater sample (bottom). Also indicated are the stable isotope values of the host calcite of the fluid-inclusion samples and the calculated temperatures from the paired fluid-inclusion and host calcite oxygen isotope ratios. This calculation is based on the (Tremaine et al., 2011) equation. DFT stands for distance from top.

Sample	DFT	$\delta^{13}C_{cc}$	$\delta^{18}O_{cc}$	$CaCO_3$ weight	Yield	Rel. yield	$\delta^{18}O_{fi}$	$\delta^{2}H_{fi}$	Calculated T
	cm	‰ VPDB	‰ VPDB	g	mL	mL g^{-1}	‰ VSMOW	‰ VSMOW	°C
2012#5	29	–	–	0.50	0.27	0.54	−4.97	−43.08	–
2012#5	20	−8.8	−4.4	0.60	0.25	0.42	−6.05	−46.66	11.1
2012#5	2	−6.7	−3.9	0.40	0.26	0.65	−5.94	−44.69	8.8
2012#5	2	−7.0	−4.2	0.40	0.20	0.50	−6.95	−47.01	5.3
2012#5	2	−6.9	−4.2	0.30	0.18	0.60	−6.04	−45.49	9.7
2012#5	25	−6.8	−3.8	0.40	0.09	0.23	−6.86	−46.42	4.1
2012#5	10	−7.8	−4.5	0.40	0.18	0.45	−4.54	−42.76	19.4
2012#5	41	−8.5	−4.6	0.50	0.40	0.80	−6.21	−43.83	10.9
2012#5	10	−7.8	−4.6	0.40	0.21	0.53	−4.88	−44.44	17.9
2012#5	5	−8.1	−4.2	0.50	0.30	0.60	−5.21	−43.12	14.0
2012#5	29	−8.5	−4.6	0.60	0.48	0.80	−5.21	−43.89	16.0
2012#5	45	−7.5	−4.2	0.46	0.21	0.46	−2.89	−39.84	26.4
2012#5	50	−8.6	−4.8	0.70	0.28	0.40	−6.41	−44.29	11.3
2012#5	45.5	−8.4	−4.6	0.72	0.20	0.28	−5.29	−41.6	15.6
2012#5	60	−7.8	−4.8	0.38	0.33	0.87	−7.04	−46.86	7.9
2012#5	70	−8.4	−4.9	0.39	0.07	0.18	−4.73	−41.35	20.5
2012#5	60	−7.6	−4.6	0.40	0.41	1.03	−6.96	−46.51	7.4
2012#5	70	−8.8	−4.9	0.57	0.14	0.25	−3.907	−40.36	25.0
2010#2	50	−8.0	−4.4	0.68	0.05	0.07	–	–	–
2010#2	7	−10.0	−5.1	0.90	0.33	0.37	−6.11	−42.12	13.9
2010#1	37	−10.3	−5.5	0.70	0.34		−6.62	−47.13	13.5
2010#2	24	−10.0	−5.3	0.81	0.29	0.36	−6.96	−44.68	10.6
2010#1	11	−8.6	−4.6	0.56	0.05	0.09	–	–	–
2010#1	27	−10.9	−5.2	0.76	0.28	0.37	−7	−44.38	10.1
2012#4	2	−9.5	−5.0	0.81	1.01	1.25	−7.67	-53.62	5.8
2012#4	8	−8.7	−4.9	0.46	1.02	2.22	−7.56	−53.8	5.8
2012#4	2	−9.7	−5.0	0.27	0.51	1.89	−7.6	−54.39	6.3
2012#4	8	−9.0	−4.9	0.33	0.54	1.64	−7.98	−55.49	3.9
2012#1	21	−7.0	−3.4	0.45	0.03	0.07	–	–	–
2012#1	2	−9.4	−4.6	0.87	0.29	0.33	−6.89	−46.43	7.8
2012#1	10	−8.6	−4.3	0.95	0.44	0.46	−6.68	−44	7.1
2012#1	21	−7.6	−3.6	0.98	0.20	0.20	−4.74	−41.09	13.3
2012#2	38	−7.4	−3.9	0.90	0.43	0.48	−6.08	−43.49	8.4
2012#2	19	−5.2	−3.2	0.89	0.31	0.35	−5.12	−41.9	9.3
2012#2	4	−9.0	−4.2	0.75	0.40	0.53	−6.78	−46.92	6.4
2012#2	31	−8.1	−4.2	0.78	0.41	0.53	−6.53	−44.01	7.4
2010#14	30	−8.6	−4.5	0.79	0.18	0.23	−4.25	−41.21	20.5
2010#14	19	−8.4	−4.7	0.88	0.15	0.17	−5.91	−44.44	13.1
2010#14[a]	22	−5.3	−3.2	0.74	0.02	0.03	–	–	–
2010#6	10	−8.8	−4.7	0.88	0.41	0.47	−6.17	−44.07	11.7
2010#6	4	−8.2	−4.1	0.80	0.22	0.28	−1.27	−37.77	35.6
2010#6	13	−7.9	−3.9	0.84	0.17	0.20	−0.65	−36.58	37.5
2010#6	6	−8.0	−4.1	0.93	0.51	0.55	−6.35	−46.06	7.6
2010#6	4	−8.1	−4.1	0.80	0.05	0.06	–	–	–
2014#618-3 base	10	−7.9	−4.1	0.80	0.44	0.55	−6.25	−44.52	8.3
2014#618-3 middle	5	−7.0	−4.3	0.79	0.56	0.71	−6.47	−44.61	8.1
2014#618-3 side[a]	–	−5.41	−3.62	0.68	0.02	0.03	–	–	–
2014#618-3 side2[b]	–	–	–	1.10	failed	–	–	–	–
2014#206	9	−7.01	−4.45	0.50	0.93	1.86	−6.75	−49.29	7.6
2014#206	2.4	−7.97	−4.88	0.50	0.64	1.28	−5.45	−47.48	16.3
Dripwater sample							−6.48	−42.40	

[a] Minor visible diagenesis is present in this sample. [b] Significant visible diagenesis is present in this sample.

of ∼ 78–74 ka at the base (corresponding to MIS-5a) and ages around 53 ka towards the top (corresponding to MIS-3). For stalagmite 2010#6, growth of particularly the older part of this specimen coincided with wetter conditions in southern Europe and the well-documented Mediterranean Sapropel S6 event that relates to a maximum in Northern Hemisphere summer insolation (Bard et al., 2002; Kroon et al., 1998; Sancho et al., 2015; Wainer et al., 2013). Stalagmite 2010#6 may suggest that these wet conditions occurred further north in Europe as well. Even though western Europe and the Mediterranean region experienced relatively wet conditions at that time, the global sea level was significantly below the modern values (Bard et al., 2002). This appears to indicate that speleothem growth in Scladina Cave did not necessarily require full interglacial settings in the past. Favorable hydrological conditions around 170–174 ka could perhaps relate to comparatively high sea surface temperatures (SSTs) at the Iberian margin at that point in time (Martrat et al., 2007). At 142 ka, the youngest age of stalagmite 2010#6 coincides with some of the lowest temperatures in MIS-6. Iberian margin SSTs are also low, coinciding with the maximum ice extent in northern Europe (Ahn et al., 2017). While we cannot discard this U–Th analysis on analytical grounds, this remains an age that we regard with some caution. Growth conditions for speleothems in Scladina Cave must have been rather unfavorable at 142 ka, and we are also not aware of other speleothem occurrences of this age in northern Europe.

Stalagmite 2014#206 is another specimen that grew under non-interglacial conditions. It has ages of ∼ 78–74 ka at the base (corresponding to MIS-5a) and ages around 53 ka towards the top (corresponding to MIS-3).

This interval is characterized by millennial-scale Dansgaard–Oeschger variability (Rasmussen et al., 2014), which is well documented in Greenland ice cores, whereby Greenland interstadials (warmer periods) would likely have been more favorable than Greenland stadials (colder periods) for speleothem growth in Scladina Cave. The oldest ages of 2014#206 correspond to the time interval of Greenland interstadial GI-21 and Greenland stadial GS-20; (Rasmussen et al., 2014), and the younger ages of 2014#206 correspond to pronounced Greenland interstadial GI-14. (Fig. 6). Regardless of their assignment to Greenland stadials or interstadials, all measured ages of speleothem 2014#206 correspond to relatively high SSTs at the Iberian margin that are to some extent decoupled from Dansgaard–Oeschger variability recorded in the NGRIP ice core for this time interval (Martrat et al., 2007). The interval around 53 ka also corresponds to a particularly clear peak in tree pollen and other forest indicators in the Eifel Maar record (Riechelmann et al., 2023). Speleothem growth occurred at several other European sites at intervals around both 76 and 53 ka (Lechleitner et al., 2018; Peral et al., 2024; Riechelmann et al., 2023).

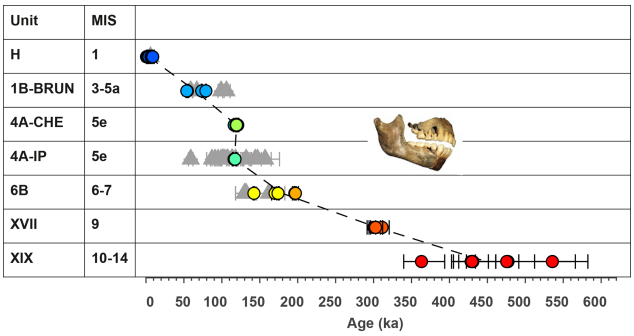

Figure 8. Schematic overview of the U–Th ages of the present study (the color scheme is the same as Fig. 6) compared with earlier U–Th ages (in gray), as summarized in Bonjean (1998). Unit numbers conform with the stratigraphic column in Fig. 3. Please note that units without U–Th ages are not shown. The dashed line connects the median values of the ages from the current study.

4.4 New U–Th ages in comparison to the existing Scladina Cave age model

The new ages we present here compare favorably to the existing age model of Scladina Cave (Fig. 8; Pirson et al., 2014b). Methodological progress made over the past decades clearly comes forward in the direct comparison to previously published U–Th ages (Bonjean, 1998; Gewelt et al., 1992) that are generally in the same range as our ages but with much larger uncertainties. Because we have more precise ages now and have provided ages in previously undated intervals, our data allow for several changes and additions to the existing age model.

First, the ages we provide for the lower part of the Scladina stratigraphic sequence chart new territory. The oldest units in the Scladina Cave sequence that we could date are from a speleothem complex in unit 6B. At an age of 197 ka, these speleothems correlate to the latest part of MIS-7, while it has previously been systematically positioned inside MIS-5 (Bastin, 1992; Bonjean, 1998; Cordy and Bastin, 1992; Pirson et al., 2014b). These new ages demonstrate that the older part of the Scladina sequence belongs to the Middle Pleistocene and more specifically to the Late Saalian.

Furthermore, the ages of the unit 4A-IP stalagmites unequivocally indicate that they grew in MIS-5e, equivalent to the Eemian period (Shackleton et al., 2003), while in the previous age model, these were attributed to MIS-5a or MIS-5c (Pirson et al., 2014b). This has implications for the currently accepted age of the Scladina 1-4A juvenile Neanderthal remains, as these were found in a unit directly overlying this stalagmitic floor. Even though the reworked nature of the Neanderthal fossils (Pirson et al., 2014a) and the lack of precision in the chronology of the sequence situated immediately above unit 4A-IP (Pirson, 2014) prevent firm conclusions, the new ages make it more plausible that the deposition of

the Neanderthal remains predate MIS-5a and more probably belong to MIS-5d.

These ages further suggest that the Middle Paleolithic assemblage from unit 5 (Bonjean et al., 2014), which so far has been dated at 130 ± 20 ka (Huxtable and Aitken, 1992) and positioned inside MIS-5 (Pirson et al., 2014b), predates MIS-5e. If we would choose to reject the 142 ka age in the top section of speleothem 2010#6 from unit 5B on the grounds that speleothem growth would have been rather unlikely in the glacial conditions that prevailed at that time, then the Middle Paleolithic assemblage from unit 5 postdates the brief climate amelioration dated at 170–174 ka in MIS-6 (as recorded in the two older ages from stalagmite 2010#6). The stratigraphical placement of the unit 5 archeological assemblage in MIS-6 (Fig. 3) is then also in good agreement with the infrared-stimulated luminescence (IRSL)-derived age of 153 ± 15 ka obtained from unit 4B overlying unit 5 (Pirson et al., 2014b). However, if the 142 ka age of the top of stalagmite 2010#6 is taken to be accurate, then the unit 5 Paleolithic assemblage would most likely have been deposited in the last and coldest part of MIS-6.

Finally, our results allow, for the first time, to assign ages to the stratigraphy of the underlying Sous-Saint-Paul Cave, showing that this sequence developed during the Middle Pleistocene. Adding the sedimentary record of the underlying Sous-Saint-Paul Cave to that of Scladina Cave extends the complete sedimentary sequence down to at least MIS-10 or perhaps even to MIS-14, which makes this one of the stratigraphically longer cave sedimentary records in northwestern Europe.

5 Conclusions

In Scladina Cave and in the underlying Sous-Saint-Paul Cave, burial of speleothems in siliciclastic sediments deposited in glacial periods has led to diagenetic alteration of speleothem calcite. Neomorphic alteration from the speleothem surface inwards leads to visible discoloration and is shown in trace element patterns. In the diagenetic process, observed mobilization of ^{238}U compromises U–Th dating of altered material. In the same process, PO_4, likely sourced from bat guano in the sediment, was mobilized and remineralized in the speleothem fabric. Regardless, the diagenetic process was not pervasive, and through careful sample screening we identified speleothem material with little to no diagenetic alteration from Sous-Saint-Paul Cave and Scladina Cave for U–Th dating. U–Th ages of these well-preserved speleothems confirm that their formation in these two connected caves predominantly occurred in warm (interglacial or interstadial) periods of the late Quaternary. Intercalated siliciclastic sediments were the dominant mode of deposition in colder periods. The data provide a robust age framework for Scladina Cave and add precisely dated stratigraphic anchor points to the younger part of the sequence that improve the previous age model. One notable consequence of the new U–Th ages is that a juvenile Neanderthal mandible, previously placed in Marine Isotope Stage 5a or 5b, could now potentially date back to Marine Isotope Stage 5d. Furthermore, new U–Th analyses provide Middle Pleistocene ages for the previously undated lower part of the Scladina sequence and the underlying Sous-Saint-Paul sequence. All ages combined suggest this system to be one of the longer fossil-rich sedimentary cave sequences in NW Europe.

Fluid-inclusion isotope analysis performed on the same material indicates that many samples are well preserved, and the measured isotope values inform us on the isotope composition of past rainfall for the Scladina site. A subset of fluid-inclusion isotope data trend away from the GMWL, which we postulate to be potentially related to diagenetic weakening of the speleothem calcite fabric. All data combined serve to remind us of the importance of careful sample selection in cave settings where burial in siliciclastic sediments has led to diagenetic overprints on speleothem calcite.

Appendix A

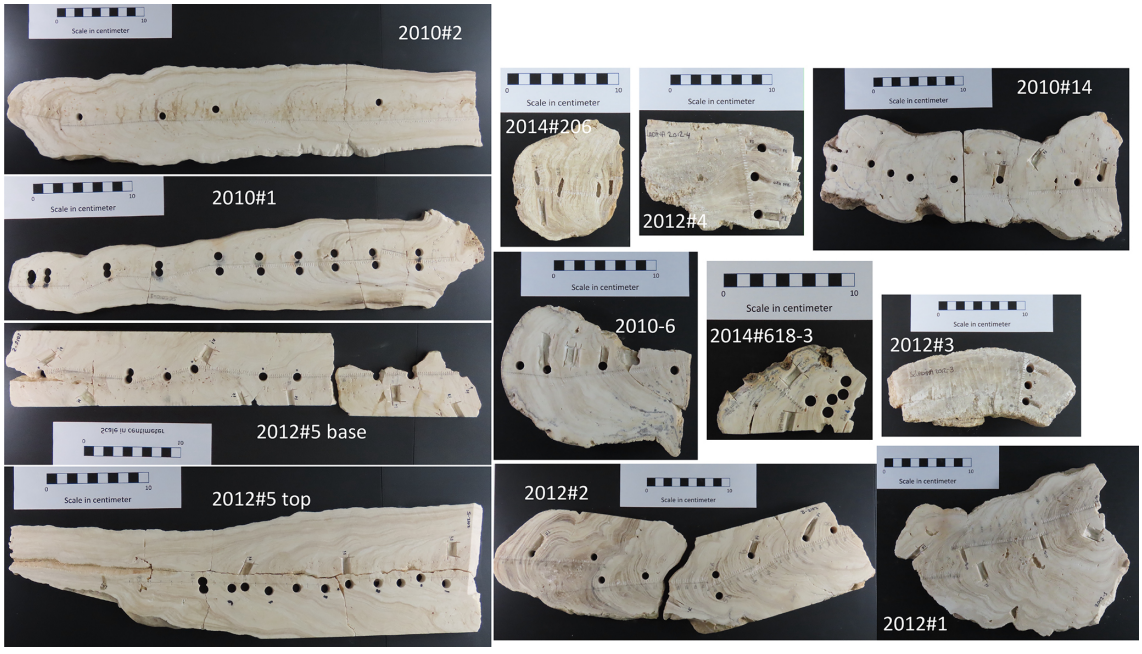

Figure A1. Overview of slabs cut from the stalagmite specimens studied. The drill holes visible on many of the slabs were made for earlier student project analyses. Precise locations of samples in the present study can be retrieved from Table 1.

Appendix B

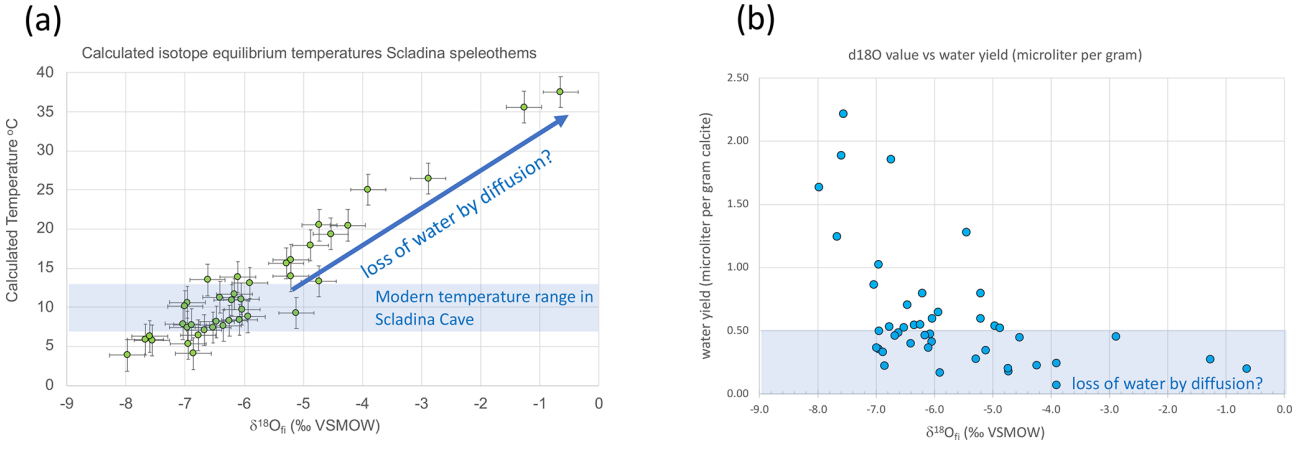

Figure B1. **(a)** Isotope equilibrium temperatures calculated from paired oxygen isotope values of fluid inclusions and their host calcite. The shaded blue box spans the modern seasonal temperature variation measured in the cave. Higher $\delta^{18}O_{fi}$ values lead to unrealistically high temperatures, suggesting that the process that leads the fluid-inclusion values away from the GMWL sends the fluid inclusions and their host calcite out of isotopic equilibrium. **(b)** Cross plot showing that lower water yield samples tend to have higher $\delta^{18}O_{fi}$ values. The blue zone indicates samples with lower than 0.5 µL per gram extraction yields, which we postulate to be the samples that may have lost water through diffusion, leading the remaining water to be isotopically fractionated towards higher $d^{18}O_{fi}$ values.

Data availability. Laser ablation trace element data used in this publication are available at https://doi.org/10.17617/3.UKDF4T (Vonhof, 2024).

Author contributions. HBV coordinated the project in which MAPvN, JR, MvdD, and DaB. performed initial lab work and analyses. Samples were collected and placed in stratigraphical context by DoB, SP, KdM, and GA. U–Th analyses were provided by JH, DS, MW, SV, HC, and XJ. Uniform age calculations based on data from all labs were provided by DS and MW. Materials for figures were provided by JLvdL, DoB, and SP. Based on in-depth discussion with SV, JLvdL, SP, and DoB, HBV prepared the manuscript with contributions from all co-authors.

Competing interests. The contact author has declared that none of the authors has any competing interests.

Disclaimer. Publisher's note: Copernicus Publications remains neutral with regard to jurisdictional claims made in the text, published maps, institutional affiliations, or any other geographical representation in this paper. While Copernicus Publications makes every effort to include appropriate place names, the final responsibility lies with the authors.

Special issue statement. This article is part of the special issue "Paleoclimate, from observing modern processes to reconstructing the past: a tribute to Dick (Dirk) Kroon". It is not associated with a conference.

Acknowledgements. This study is the cumulative result of many years of research effort of students at Vrije Universiteit Amsterdam and later at the Max Planck Institut für Chemie and the Johannes Gutenberg Universität, Mainz. This project would not even have started if it were not for the enthusiastic support by Dick Kroon, at that point in time Professor at the Earth Sciences Department at Vrije Universiteit Amsterdam. With his broad interest in new paleoceanographical and paleoclimatological proxy systems and techniques, Dick motivated and supported Hubert Vonhof to initiate the speleothem paleoclimate research that has remained one of Hubert's key scientific topics in the years that followed.

Special acknowledgement goes to Laura García Soler, one of the students that contributed to this study. We have unfortunately not been able to reach her to offer co-authorship on this paper.

Financial support. The article processing charges for this open-access publication were covered by the Max Planck Society.

Review statement. This paper was edited by Simon Jung and reviewed by two anonymous referees.

References

Ahn, S., Khider, D., Lisiecki, L. E., and Lawrence, C. E.: A probabilistic Pliocene–Pleistocene stack of benthic $\delta^{18}O$ using a profile hidden Markov model, Dynamics and Statistics of the Climate System, 2, dzx002, https://doi.org/10.1093/climsys/dzx002, 2017.

Audra, P., Heresanu, V., Barriquand, L., El Kadiri Boutchich, M., Jaillet, S., Pons-Branchu, E., Bosak, P., Cheng, H., Edwards, R. L., and Renda, M.: Bat guano minerals and mineralization processes in Chameau Cave, Eastern Morocco, Int. J. Speleol., 50, 91–109, https://doi.org/10.5038/1827-806x.50.1.2374, 2021.

Bajo, P., Hellstrom, J., Frisia, S., Drysdale, R., Black, J., Woodhead, J., Borsato, A., Zanchetta, G., Wallace, M. W., Regattieri, E., and Haese, R.: "Cryptic" diagenesis and its implications for speleothem geochronologies, Quaternary Sci. Rev., 148, 17–28, https://doi.org/10.1016/j.quascirev.2016.06.020, 2016.

Bard, E., Antonioli, F., and Silenzi, S.: Sea-level during the penultimate interglacial period based on a submerged stalagmite from Argentarola Cave (Italy), Earth Planet. Sc. Lett., 196, 135–146, https://doi.org/10.1016/s0012-821x(01)00600-8, 2002.

Bastin, B.: Analyse pollinique des sédiments détritiques, des coprolithes et des concretions du site préhistorique de la grotte Scladina (Province de Namur, Belgique), in: Recherches aux grottes de Sclayn Vol. 1, Le contexte, edited by: Otte, M., Etudes et recherches Archeologiques de l'Université de Liège, 27, Universite de Liège, Liége, 59–77, Université de Liège, Liège, ISBN 978-2-930495-23-1, 1992.

Bocherens, H.: Diet and ecology of the Scladina 1-4A Neandertal child: insights from stable isotopes, in: The Scladina I-4A juvenile Neandertal, edited by: Toussaint, M., and Bonjean, D., Études et recherches archéologiques de l'Université de Liège, 134, ERAUL, Liège, 351–362, ISBN 978-2-930495-20-0, 2014.

Bocherens, H., Billiou, D., Patou-Mathis, M., Bonjean, D., Otte, M., and Mariotti, A.: Paleobiological implications of the isotopic signatures (^{13}C, ^{15}N) of fossil mammal collagen in Scladina cave (Sclayn, Belgium), Quaternary Res., 48, 370–380, https://doi.org/10.1006/qres.1997.1927, 1997.

Bonjean, D.: Chronologie à la grotte Scladina, in: Recherches aux grottes de Sclayn, vol. 2, l'Archéologie, edited by: Otte, M., Patou-Mathis, M., and Bonjean, D., Études et recherches archéologiques de l'Université de Liège, 134, ERAUL, Liège, 45–57, 1998.

Bonjean, D., Toussaint, M., and Otte, M.: Scladina (Sclayn, Belgique): l'homme de néandertal retrouvé!, Notae Praehistoricae, 16, 37–46, 1996.

Bonjean, D., Abrams, G., Di Modica, K., Otte, M., Pirson, S., and Toussaint, M.: Scladina Cave: Archeological context and history of the discoveries, in: The Scladina I-4A juvenile Neandertal, edited by: Toussaint, M. and Bonjean, D., Études et recherches archéologiques de l'Université de Liège, 134, ERAUL, Liège, 31–48, ISBN 978-2-930495-20-0, 2014.

Cheng, H., Edwards, R. L., Shen, C. C., Polyak, V. J., Asmerom, Y., Woodhead, J., Hellstrom, J., Wang, Y. J., Kong, X. G., Spotl, C., Wang, X. F., and Alexander, E. C.: Improvements in ^{230}Th dating, ^{230}Th and ^{234}U half-life values, and U–Th isotopic measurements by multi-collector inductively coupled plasma mass spectrometry, Earth Planet. Sc. Lett., 371, 82–91, https://doi.org/10.1016/j.epsl.2013.04.006, 2013.

Cheng, H., Zhang, H., Spötl, C., Baker, J., Sinha, A., Li, H., Bartolomeì, M., Moreno, A., Kathayat, G., Zhao, J., Dong, X., Li, Y., Ning, Y., Jia, X., Zong, B., Ait Brahim, Y., Pérez-Mejìas, C., Cai, Y., Novello, V. F., Cruz, F. W., Severinghaus, J. P., An, Z., and Edwards, R. L.: Timing and structure of the Younger Dryas event and its underlying climate dynamics, P. Natl. Acad. Sci. USA, 117, 23408–23417, https://doi.org/10.1073/pnas.2007869117, 2020.

Cordy, J.-M. and Bastin, B.: Synthe`se des études paléontologiques realisées dans les dépôts de la grotte Scladina (Sclayn, Province de de Namur), in: Recherches aux grottes de Sclayn Vol. 1, Le contexte, edited by: Otte, M., Etudes et recherches Archeologiques de l'Université de Liège, 27, Universite de Liège, Liége, ISBN 978-2-930495-23-1, 1992.

de Graaf, S., Vonhof, H. B., Weissbach, T., Wassenburg, J. A., Levy, E. J., Kluge, T., and Haug, G. H.: A comparison of isotope ratio mass spectrometry and cavity ring-down spectroscopy techniques for isotope analysis of fluid inclusion water, Rapid Commun. Mass Sp., 34, e8837, https://doi.org/10.1002/rcm.8837, 2020.

Dennis, P. F., Rowe, P. J., and Atkinson, T. C.: The recovery and isotopic measurement of water from fluid inclusions in speleothems, Geochim. Cosmochim. Ac., 65, 871–884, https://doi.org/10.1016/S0016-7037(00)00576-7, 2001.

Fernandez, A., Løland, M. H., Maccali, J., Krüger, Y., Vonhof, H. B., Sodemann, H., and Meckler, A. N.: Characterization and Correction of Evaporative Artifacts in Speleothem Fluid Inclusion Isotope Analyses as Applied to a Stalagmite From Borneo, Geochem. Geophy. Geosy., 24, e2023GC010857, https://doi.org/10.1029/2023GC010857, 2023.

Frisia, S.: Microstratigraphic logging of calcite fabrics in speleothems as tool for palaeoclimate studies, Int. J. Speleol., 44, 1–16, https://doi.org/10.5038/1827-806x.44.1.1, 2015.

Frisia, S., Borsato, A., Fairchild, I. J., and McDermott, F.: Calcite fabrics, growth mechanisms, and environments of formation in speleothems from the Italian Alps and southwestern Ireland, J. Sediment Res., 70, 1183–1196, https://doi.org/10.1306/022900701183, 2000.

Gewelt, M., Schwarcz, H. P., and Szabo, B. J.: Datations $^{230}Th/^{234}U$ et 14C de concrétions stalagmitiques de la grotte Scladina, in: Recherches aux grottes de Sclayn Vol. 1, Le contexte, edited by Otte, M., Etudes et recherches Archeologiques de l'Université de Liège, 27, Universite de Liège, Liége, 159–172, ISBN 978-2-930495-23-1, 1992.

Hellstrom, J.: Rapid and accurate U/Th dating using parallel ion-counting multi-collector ICP-MS, J. Anal. Atom. Spectrom, 18, 1346–1351, https://doi.org/10.1039/b308781f, 2003.

Huxtable, J. and Aitken, M. J.: Thermoluminescence dating of burned flint and stalagmitic calcite from grottes de Sclayn (Namur), in: Recherches aux grottes de Sclayn, Vol. 1, Le contexte, edited by: Otte, M., Etudes et recherches Archeologiques de l'Université de Liège, 27, Universite de Liège, Liége, 175–178, ISBN 978-2-930495-23-1, 1992.

IAEA/WMO: Global Network of Isotopes in Precipitation, The GNIP Database, https://nucleus.iaea.org/wiser (last access: 17 November 2023), 2023.

Jochum, K. P., Scholz, D., Stoll, B., Weis, U., Wilson, S. A., Yang, Q., Schwalb, A., Börner, N., Jacob, D. E., and Andreae, M. O.: Accurate trace element analysis of speleothems and biogenic calcium carbonates by LA-ICP-MS, Chem. Geol., 318–319, 31–44, https://doi.org/10.1016/j.chemgeo.2012.05.009, 2012.

KMI: Klimaatstatistieken van de Belgische gemeenten, https://www.meteo.be/nl/klimaat/klimaat-van-belgie/klimaat-in-uw-gemeente (last access: 20 June 2024), 2024.

Kroon, D., Alexander, I. T., Little, M. G., Lourens, L. J., Matthewson, A., Robertson, A. H. F., and Sakamoto, T.: Stable isotope record and age model for sapropel stratigraphy of ODP Site 160-967, PANGAEA [data set], https://doi.org/10.1594/PANGAEA.790405, 1998.

Lechleitner, F. A., Amirnezhad-Mozhdehi, S., Columbu, A., Comas-Bru, L., Labuhn, I., Pérez-Mejías, C., and Rehfeld, K.: The Potential of Speleothems from Western Europe as Recorders of Regional Climate: A Critical Assessment of the SISAL Database, Quaternary, 1, 1–30, https://doi.org/10.3390/quat1030030, 2018.

Lisiecki, L. E. and Raymo, M. E.: A Pliocene-Pleistocene stack of 57 globally distributed benthic $\delta^{18}O$ records, Paleoceanography, 20, 1–17, https://doi.org/10.1029/2004pa001071, 2005.

Martrat, B., Grimalt, J. O., Shackleton, N. J., de Abreu, L., Hutterli, M. A., and Stocker, T. F.: Four Climate Cycles of Recurring Deep and Surface Water Destabilizations on the Iberian Margin, Science, 317, 502–507, https://doi.org/10.1126/science.1139994, 2007.

Obert, J. C., Scholz, D., Felis, T., Brocas, W. M., Jochum, K. P., and Andreae, M. O.: $^{230}Th/U$ dating of Last Interglacial brain corals from Bonaire (southern Caribbean) using bulk and theca wall material, Geochim. Cosmochim. Ac., 178, 20–40, https://doi.org/10.1016/j.gca.2016.01.011, 2016.

Orlando, L., Darlu, P., Toussaint, M., Bonjean, D., Otte, M., and Hanni, C.: Revisiting Neandertal diversity with a 100,000 year old mtDNA sequence, Curr. Biol., 16, R400–R402, https://doi.org/10.1016/j.cub.2006.05.019, 2006.

Otte, M. (Ed.): Recherches aux grottes de Sclayn. Volume 1: Le contexte, Etudes et Recherches archéologiques de l'Université de Liège, 1, l'Université de Liège, Liege, 178 pp., ISBN 978-2-930495-23-1, 1992.

Otte, M., Toussaint, M., and Bonjean, D.: Découverte de restes humains immatures dans les niveaux moustériens de la grotte Scladina à Andenne (Belgique), B. Mém. Soc. Anthro. Par., 5, 327–332, 1993.

Peral, M., Marchegiano, M., Verheyden, S., Goderis, S., Van Helden, T., Vanhaecke, F., Van Acker, T., Jia, X., Cheng, H., Fiebig, J., Fourcade, T., Snoeck, C., and Claeys, P.: A new insight of the MIS 3 Dansgaard-Oeschger climate oscillations in western Europe from the study of a Belgium isotopically equilibrated speleothem, Quaternary Sci. Rev., 329, 108564, https://doi.org/10.1016/j.quascirev.2024.108564, 2024.

Peyregne, S., Slon, V., Mafessoni, F., de Filippo, C., Hajdinjak, M., Nagel, S., Nickel, B., Essel, E., Le Cabec, A., Wehrberger, K., Conard, N. J., Kind, C. J., Posth, C., Krause, J., Abrams, G., Bonjean, D., Di Modica, K., Toussaint, M., Kelso, J., Meyer, M., Paabo, S., and Prufer, K.: Nuclear DNA from two early Neandertals reveals 80,000 years of genetic continuity in Europe, Sci. Adv., 5, eaaw5873, https://doi.org/10.1126/sciadv.aaw5873, 2019.

Pirson, S.: Contribution à l'étude des dépôts d'entrée de grotte en Belgique au Pléistocène supérieur. Stratigraphie, sédimento-

genèse et paléoenvironnement, PhD thesis, Univerity of Liège and Royal Belgian Institute of Natural Sciences, 435 pp., 2007.

Pirson, S.: The stratigraphic sequence of Scladina Cave, in: The Scladina I-4A juvenile Neandertal, edited by: Toussaint, M., and Bonjean, D., Études et recherches archéologiques de l'Université de Liège, 134, ERAUL, Liège, 69–92, ISBN 978-2-930495-20-0, 2014.

Pirson, S., Court-Picon, M., Haesaerts, P., Bonjean, D., and Damblon, F.: New data on geology, anthracology and palynology from the Scladina Cave Pleistocene sequence: preliminary results, Memoirs of the Geological Survey of Belgium, 55, 71–93, 2008.

Pirson, S., Bonjean, D., and Toussaint, M.: Stratigraphic origin of the juvenile Neandertal remains from Scladina Cave: re-evaluation and consequences for their palaeoenvironmental and chronostratigraphic contexts, in: The Scladina I-4A juvenile Neandertal, edited by: Toussaint, M., and Bonjean, D., Études et recherches archéologiques de l'Université de Liège, 134, ERAUL, Liège, 93–115, ISBN 978-2-930495-20-0, 2014a.

Pirson, S., Court-Picon, M., Damblon, F., Balescu, S., Bonjean, D., and Haesaerts, P.: The paleoenvironmental context and chronostratigraphic frameworkof the Scladina Cave sedimentary sequence (units 5 to 3-sup), in: The Scladina I-4A juvenile Neandertal, edited by: Toussaint, M., and Bonjean, D., Études et recherches archéologiques de l'Université de Liège, 134, ERAUL, Liège, 69–92, ISBN 978-2-930495-20-0, 2014b.

Quinif, Y.: Complex stratigraphic sequences in Belgian caves correlation with climatic changes during the Middle, the Upper Pleistocene and the Holocene, Geol. Belg., 9, 231–244, 2006.

Rasmussen, S. O., Bigler, M., Blockley, S. P., Blunier, T., Buchardt, S. L., Clausen, H. B., Cvijanovic, I., Dahl-Jensen, D., Johnsen, S. J., Fischer, H., Gkinis, V., Guillevic, M., Hoek, W. Z., Lowe, J. J., Pedro, J. B., Popp, T., Seierstad, I. K., Steffensen, J. P., Svensson, A. M., Vallelonga, P., Vinther, B. M., Walker, M. J. C., Wheatley, J. J., and Winstrup, M.: A stratigraphic framework for abrupt climatic changes during the Last Glacial period based on three synchronized Greenland ice-core records: refining and extending the INTIMATE event stratigraphy, Quaternary Sci. Rev., 106, 14–28, https://doi.org/10.1016/j.quascirev.2014.09.007, 2014.

Riechelmann, D. F. C., Albert, J., Britzius, S., Krebsbach, F., Scholz, D., Schenk, F., Jochum, K. P., and Sirocko, F.: Bioproductivity and vegetation changes documented in Eifel maar lake sediments (western Germany) compared with speleothem growth indicating three warm phases during the last glacial cycle, Quatern. Int., 673, 1–17, https://doi.org/10.1016/j.quaint.2023.11.001, 2023.

Sancho, C., Arenas, C., Vázquez-Urbez, M., Pardo, G., Lozano, M. V., Peña-Monné, J. L., Hellstrom, J., Ortiz, J. E., Osácar, M. C., Auqué, L., and Torres, T.: Climatic implications of the Quaternary fluvial tufa record in the NE Iberian Peninsula over the last 500 ka, Quaternary Res., 84, 398–414, https://doi.org/10.1016/j.yqres.2015.08.003, 2015.

Scholz, D. and Hoffmann, D.: ^{230}Th/U-dating of fossil corals and speleothems, Quaternary Sci. J., 57, 52–76, 2008.

Scholz, D., Tolzmann, J., Hoffmann, D. L., Jochum, K. P., Spötl, C., and Riechelmann, D. F. C.: Diagenesis of speleothems and its effect on the accuracy of ^{230}Th/U-ages, Chem. Geol., 387, 74–86, https://doi.org/10.1016/j.chemgeo.2014.08.005, 2014.

Seierstad, I. K., Abbott, P. M., Bigler, M., Blunier, T., Bourne, A. J., Brook, E., Buchardt, S. L., Buizert, C., Clausen, H. B., Cook, E., Dahl-Jensen, D., Davies, S. M., Guillevic, M., Johnsen, S. J., Pedersen, D. S., Popp, T. J., Rasmussen, S. O., Severinghaus, J. P., Svensson, A., and Vinther, B. M.: Consistently dated records from the Greenland GRIP, GISP2 and NGRIP ice cores for the past 104 ka reveal regional millennial-scale δ^{18}O gradients with possible Heinrich event imprint, Quaternary Sci. Rev., 106, 29–46, https://doi.org/10.1016/j.quascirev.2014.10.032, 2014.

Shackleton, N. J., Sánchez-Goñi, M. F., Pailler, D., and Lancelot, Y.: Marine Isotope Substage 5e and the Eemian Interglacial, Global Planet. Change, 36, 151–155, https://doi.org/10.1016/s0921-8181(02)00181-9, 2003.

Toussaint, M. and Bonjean, D. (Eds.): The Scladina I-4A juvenile Neandertal (Andenne, Belgium). Palaeoanthropology and Context, Etudes et Recherches archéologiques de l'Université de Liège, 134, ERAUL, Liège, 464 pp., ISBN 978-2-930495-20-0, 2014.

Tremaine, D. M., Froelich, P. N., and Wang, Y.: Speleothem calcite farmed in situ: Modern calibration of δ^{18}O and δ^{13}C paleoclimate proxies in a continuously-monitored natural cave system, Geochim. Cosmochim. Ac., 75, 4929–4950, https://doi.org/10.1016/j.gca.2011.06.005, 2011.

Uemura, R., Kina, Y., Shen, C.-C., and Omine, K.: Experimental evaluation of oxygen isotopic exchange between inclusion water and host calcite in speleothems, Clim. Past, 16, 17–27, https://doi.org/10.5194/cp-16-17-2020, 2020.

van Breukelen, M. R., Vonhof, H. B., Hellstrom, J. C., Wester, W. C. G., and Kroon, D.: Fossil dripwater in stalagmites reveals Holocene temperature and rainfall variation in Amazonia, Earth Planet. Sc. Lett., 275, 54–60, https://doi.org/10.1016/j.epsl.2008.07.060, 2008.

Vonhof, H.: Speleothem calcite trace element data, Edmond [data set], https://doi.org/10.17617/3.UKDF4T, 2024.

Wainer, K., Genty, D., Blamart, D., Bar-Matthews, M., Quinif, Y., and Plagnes, V.: Millennial climatic instability during penultimate glacial period recorded in a south-western France speleothem, Palaeogeogr. Palaeocl., 376, 122–131, https://doi.org/10.1016/j.palaeo.2013.02.026, 2013.

Wedepohl, H. K.: The composition of the continental crust, Geochim. Cosmochim. Ac., 59, 1217–1232, https://doi.org/10.1016/0016-7037(95)00038-2, 1995.

Weij, R., Sniderman, J. M. K., Woodhead, J. D., Hellstrom, J. C., Brown, J. R., Drysdale, R. N., Reed, E., Bourne, S., and Gordon, J.: Elevated Southern Hemisphere moisture availability during glacial periods, Nature, 626, 319–326, https://doi.org/10.1038/s41586-023-06989-3, 2024.

Yang, Q., Scholz, D., Jochum, K. P., Hoffmann, D. L., Stoll, B., Weis, U., Schwager, B., and Andreae, M. O.: Lead isotope variability in speleothems – A promising new proxy for hydrological change? First results from a stalagmite from western Germany, Chem. Geol., 396, 143–151, https://doi.org/10.1016/j.chemgeo.2014.12.028, 2015.